Russian Geology and Geophysics © 2020, V.S. Sobolev IGM, Siberian Branch of the RAS
Vol. 61, No. 9, pp. 951–963, 2020 *DOI:10.15372/RGG2019138* *Geologiya i Geofizika*

Early Proterozoic Basic Magmatism in the South Siberian Postcollisional Magmatic Belt (by the Example of the Ust'-Ignok Massif in the Urik–Iya Graben)

T.V. Donskaya[a, ✉], D.P. Gladkochub[a], A.M. Mazukabzov[a], E.N. Lepekhina[b], P.A. L'vov[b], E.I. Demonterova[a], Z.L. Motova[a]

[a] *Institute of the Earth's Crust, Siberian Branch of the Russian Academy of Sciences, ul. Lermontova 128, Irkutsk, 664033, Russia*

[b] *A.P. Karpinsky Research Russian Geological Institute, Srednii pr. 74, St. Petersburg, 199106, Russia*

Received 15 March 2019; received in revised form 28 May 2019; accepted 28 August 2019

Abstract—We performed geological, geochronological, geochemical, and isotope-geochemical studies of igneous rocks of the Ust'-Ignok gabbrodiorite massif in the Urik–Iya graben of the Siberian craton and summarized the obtained and published data on early Proterozoic mafic igneous rocks in the South Siberian postcollisional magmatic belt. It has been established that the Ust'-Ignok massif is composed of rocks of the continuous series from biotite gabbro via gabbrodiorites and diorites to quartz diorites. U–Pb zircon dating of quartz diorites of the Ust'-Ignok massif yielded an age of 1836 ± 10 Ma, i.e., the massif rocks might have originated at the final stage of the formation of the South Siberian postcollisional magmatic belt. The rocks of the Ust'-Ignok massif are of normal and medium alkalinity. All igneous rocks from gabbro to quartz diorites show distinct negative anomalies of Nb–Ta and Ti in their multielement patterns, and their $\varepsilon_{Nd}(T)$ values vary from +0.3 to –0.9. The geochemical indicator ratios in the gabbroids point to insignificant contamination of their source with continental-crust material and to their formation through the melting of an enriched lithospheric-mantle source. Gabbrodiorites–quartz diorites of the Ust'-Ignok massif resulted, most likely, from the fractional crystallization of gabbroids. Analysis of the geochemical and isotope characteristics of mafic igneous rocks of the South Siberian postcollisional magmatic belt shows that most of them resulted from the melting of the subcontinental lithospheric mantle with suprasubductional geochemical features. This mantle might have formed during subduction processes preceding the formation of the Siberian craton.

Keywords: Gabbro; diorite; U–Pb zircon age; geochemistry; Nd isotope data; early Proterozoic; Siberian craton

INTRODUCTION

The South Siberian postcollisional magmatic belt is one of major structures of the Siberian craton and extends for ~2500 km along its southern margin (Fig. 1) (Larin et al., 2003). The igneous rocks of this belt are dated at 1.88–1.84 Ga and mark the final formation of the Siberian craton as a single structure; their age also suggests that the belt was part of the Columbia supercontinent (Larin et al., 2003; Didenko et al., 2009). The belt rocks are predominantly granitoids and associated felsic volcanics; igneous rocks of mafic–intermediate composition are subordinate and occur within the South Siberian belt (Fig. 1). In particular, occasional dolerite dikes were found in the Biryusa, Sharyzhalgai, and Baikal basement salients and on the Aldan Shield (Gladkochub et al., 2010, 2012, 2013; Shokhonova et al., 2010; Popov et al., 2012; Ernst et al., 2016; Mekhonoshin et al., 2016; Donskaya et al., 2019; Ivanov et al., 2019). Gabbroids of the large Chinei massif (1.87 Ga) are localized in the Chara–Olekma terrane (Gongalsky et al., 2008a,b, 2016; Popov et al., 2009). In the Baikal salient, basaltoids are present among volcanics of the Akitkan Group of the North Baikal volcanoplutonic belt (Neimark et al., 1998; Shokhonova et al., 2010). The sources of most granitoids and felsic volcanics of the South Siberian postcollisional magmatic belt contained mantle material (Donskaya et al., 2005, 2008; Turkina et al., 2006; Turkina and Kapitonov, 2017); therefore, any information about mafic igneous rocks as potential suppliers of this material is of great importance.

In this work we present results of petrographic, geochronological, geochemical, and isotope studies of gabbroids–diorites of the unstudied Ust'-Ignok massif located in the Urik–Iya graben of the southern Siberian craton. A special goal is to summarize our and published data on the early Proterozoic mafic igneous rocks of the South Siberian postcollisional magmatic belt, to analyze the composition of their mantle sources, and to describe the potential sources of mantle material present in the zone of granitoid magma generation.

GEOLOGIC STRUCTURE OF THE STUDY AREA

The Urik–Iya graben, located between the Sharyzhalgai and Biryusa basement salients, is one of major structures of

✉ Corresponding author.
E-mail address: tatiana_donskaya@mail.ru (T.V. Donskaya)

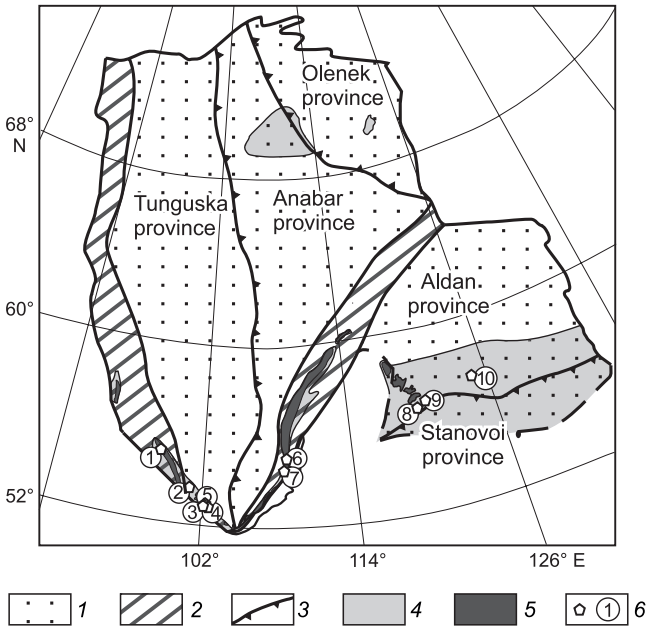

Fig. 1. Schematic tectonic map of the Siberian craton and position of the South Siberian postcollisional magmatic belt, modified after Rosen (2003), Larin et al. (2003), and Gladkochub et al. (2006). *1,* major provinces (superterranes); *2*, early Proterozoic orogenic belts; *3*, suture zones; *4*, basement salients; *5*, early Proterozoic South Siberian postcollisional magmatic belt; *6*, outcrops of early Proterozoic mafic igneous rocks. Encircled numerals: 1, dolerites and mafic volcanics of the Mal'tsev Formation of the Sayan–Biryusa volcanoplutonic belt of the Biryusa salient; 2, gabbroids of the Ust'-Ignok massif of the Urik–Iya graben; 3, dike gabbrodolerites of the Sharyzhalgai salient in the Kitoi River area; 4, gabbroids of the Malyi Zadoi massif of the Sharyzhalgai salient; 5, dolerites and lamprophyres of small massifs of the Sharyzhalgai salient in the Kitoi River area; 6, Akitkan Group basaltoids of the North Baikal volcanoplutonic belt of the Baikal salient; 7, dike dolerites of the North Baikal volcanoplutonic belt of the Baikal salient; 8, gabbroids of the Chinei complex of the Aldan Shield; 9, dike dolerites and gabbrodolerites of the Kuranakh complex of the Aldan Shield; 10, dike dolerites and gabbrodolerites of the Kalar–Nimnyr complex of the Aldan Shield.

the southern flank of the Siberian craton for studying early Proterozoic postcollisional magmatism (Fig. 2). Formation of its rocks began in an extension setting at ~1.91 Ga. This extension was due to the collapse of the orogen resulted from the collision of the Biryusa and Sharyzhalgai terranes (Gladkochub et al., 2014; Donskaya et al., 2018). The collision led to the intrusion of igneous rocks of the South Siberian postcollisional magmatic belt, mostly granitoids (Gladkochub et al., 2014). Most of the postcollisional granitoids are localized in the southwestern and southern parts of the graben, where they intrude the sediments of the Lower Bol'shaya Rechka Formation (an analogue of the Ingashi Formation located in the northeastern part of the graben) (Fig. 2). The U–Pb age of postcollisional granitoids in different massifs of the Urik–Iya graben varies from 1875 ± 8 to 1827 ± 6 Ma (Galimova et al., 2012), i.e., they are coeval with igneous rocks of the entire South Siberian postcollisional magmatic belt.

The Ust'-Ignok massif is located in the central part of the Urik–Iya graben, near the mouth of the Ignok River flowing into the Oka River (Fig. 3). The massif is composed mostly of igneous rocks of mafic–intermediate composition, which intrude the volcanosedimentary deposits of the Lower Daldarma Subformation composing the middle section of the Urik–Iya graben (Fig. 3). The massif is less than 20 km^2 in area (Galimova et al., 2012).

GEOLOGY AND PETROGRAPHY OF THE UST'-IGNOK MASSIF ROCKS

Comprehensive study of rocks of the Ust'-Ignok gabbro-diorite massif was carried out on the left bank of the Oka River, on both sides of the mouth of the Ignok River (Fig. 3). The massif is composed of rocks of the continuous series from biotite gabbro via gabbrodiorites and diorites to quartz diorites. The rocks are intruded by aplite veins. There is also a body of medium-grained gabbroids having no direct contact with the other massif rocks. These gabbroids might belong to the first phase of the Ust'-Ignok massif, but with the same probability they might be both xenoliths and younger cutting bodies, because their age is unknown and their geochemical characteristics differ from those of the other massif rocks (Donskaya et al., 2018). In this paper we do not consider aplites and gabbroids with an inexplicit geologic position.

A distinctive feature of all analyzed igneous rocks of the Ust'-Ignok massif, from gabbro to quartz diorites, is the presence of biotite (3–9%) as an accessory mineral.

In mineral composition gabbroids of the Ust'-Ignok massif correspond to biotite gabbro with partly saussuritized plagioclase, clinopyroxene, and hornblende as major minerals. Orthopyroxene, biotite, ore mineral, quartz, and K-feldspar are accessory minerals. Orthopyroxene and clinopyroxene are intimately intergrown and are overgrown with hornblende, which is replaced by tremolite–actinolite aggregate, chlorite, and epidote. Biotite in gabbro is partly replaced by chlorite and contains fine inclusions of rutile. Minor K-feldspar (2–3%) is also found in the rocks. Scarce microgranophyric intergrowths of quartz and plagioclase are observed at the K-feldspar–plagioclase boundary. Apatite is one more accessory mineral in the gabbroids.

Plagioclase and hornblende are major minerals of gabbro-diorites, diorites, and quartz diorites of the Ust'-Ignok massif; they are found in different contents. All rocks contain biotite, quartz, K-feldspar, and ore mineral as accessory minerals; gabbro, diorites, and quartz diorites with SiO_2 < 62 wt.% additionally contain clinopyroxene. We observed a decrease in the contents of hornblende (from 40 to 10%) and clinopyroxene (from 5% to 0) and an increase in the contents of plagioclase (from 35 to 60%), quartz (from 2 to 10%), and K-feldspar (from 3 to 8%) in the series gabbro-diorites–diorites–quartz diorites. The rocks underwent secondary alteration expressed as plagioclase saussuritization,

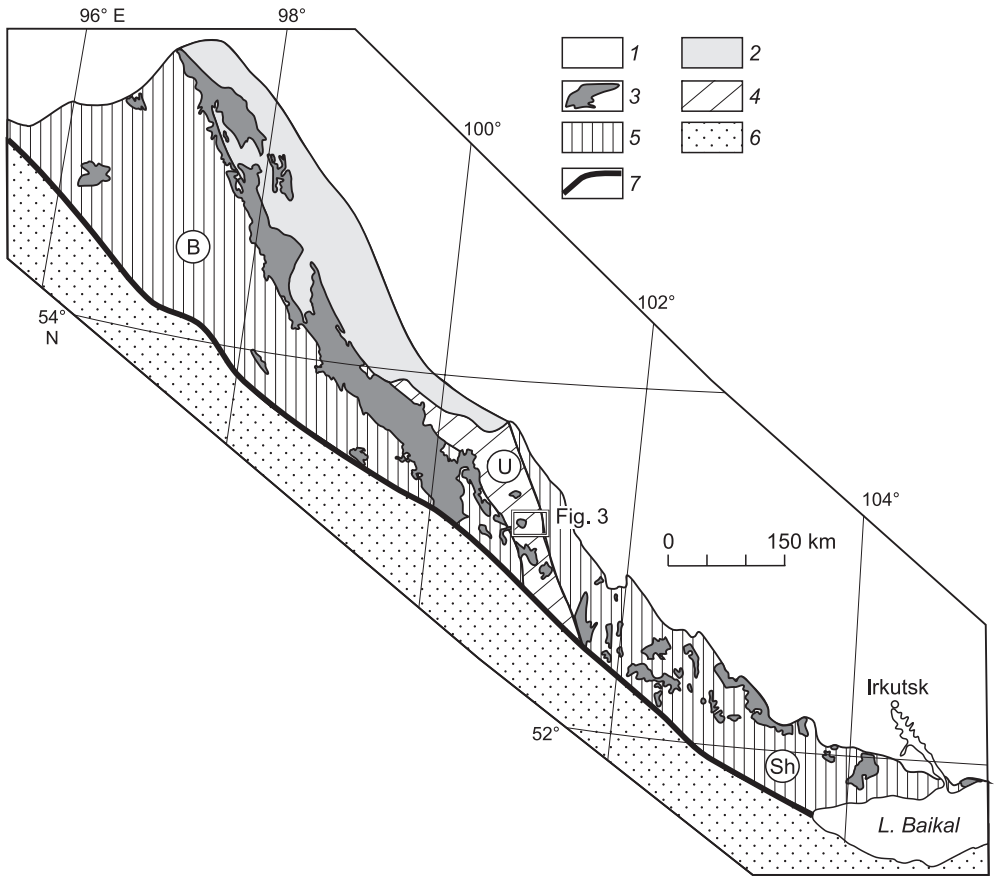

Fig. 2. Geologic structure of the southern Siberian craton, modified after Gladkochub et al. (2014). *1*, Phanerozoic sedimentary cover; *2*, deposits of the Neoproterozoic margin of the craton; *3*, early Proterozoic igneous rocks of the South Siberian postcollisional magmatic belt; *4*, early Proterozoic Urik–Iya graben (U); *5,* early Precambrian basement salients (B, Biryusa; Sh, Sharyzhalgai); *6*, Central Asian Orogenic Belt; *7*, Major Sayan Fault.

replacement of clinopyroxene by hornblende, and subsequent replacement of the hornblende by biotite and epidote. There are also chlorite and epidote pseudomorphs developed after biotite. All rocks contain apatite and sphene as accessory minerals; diorites and quartz diorites additionally contain zircon.

METHODS

Fifteen samples of igneous rocks from the Ust'-Ignok massif were analyzed for major, trace, and rare-earth elements. Three of them were dated by the Sm–Nd method, and quartz diorite was dated by the U–Pb zircon method. The site of sampling for a geochronological study is shown in Fig. 3.

Analysis for major elements was carried out by the "wet chemistry" method at the Center for Geodynamics and Geochronology of the Institute of the Earth's Crust (CGG IEC), Irkutsk (analyst E.G. Koltunova). The contents of trace and rare-earth elements were determined by ICP MS on an Agilent 7500ce (Agilent Technologies Inc., USA) quadrupole mass spectrometer at the Ultramicroanalysis Collective Instrumental Center of the Limnological Institute, Irkutsk (analyst S.V. Panteeva). The contents of elements in the samples were calculated relative to the BHVO-2, BCR-2, G-2, and GSP-2 international rock standards. Samples for an ICP MS analysis were digested by fusion with lithium metaborate according to the technique of Panteeva et al. (2003) at the CGG IEC, which ensured complete dissolution of all minerals. The error in ICP MS determination of trace and rare-earth elements did not exceed 5%.

The Sm–Nd isotope studies were carried out at the IEC. The Nd and Sm isotope ratios were measured on a Finnigan MAT-262 multicollector mass spectrometer in the static mode at the CGG IEC. The $^{143}Nd/^{144}Nd$ ratios were normalized to $^{146}Nd/^{144}Nd = 0.7219$. The 2s error in MS determination was 0.5% for Sm and Nd contents and $^{147}Sm/^{144}Nd$ and 0.005% for $^{143}Nd/^{144}Nd$. The weighted mean value of $^{143}Nd/^{144}Nd$ in the JNd-1 standard was 0.512081 ± 0.000005 (2σ, $n = 6$) in the period of measurements. The $\varepsilon_{Nd}(T)$ values and $T_{Nd}(DM)$ model ages were calculated using the modern values for the chondrite uniform reservoir (CHUR) (Jacobsen and Wasserburg, 1984) and depleted mantle (DM) (Goldstein and Jacobsen, 1988).

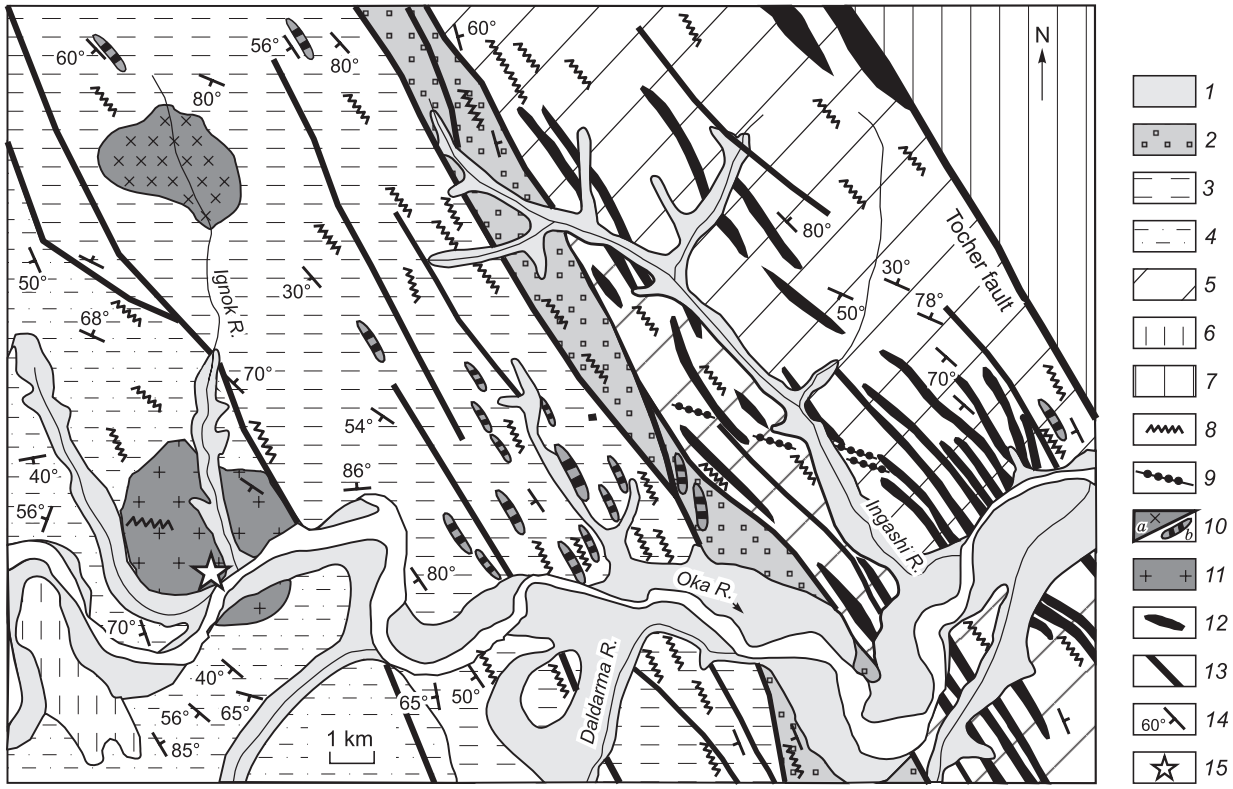

Fig. 3. Geologic structure of the central Urik–Iya graben (Ingashi–Ignok interfluve), modified after Gladkochub et al. (2014) and Donskaya et al. (2018). *1,* Quaternary alluvium; *2–6,* Urik–Iya graben sediments: *2,* Ermosokha Formation, *3, U*pper Daldarma Subformation, *4*, Lower Daldarma Subformation, *5,* Ingashi Formation, *6,* Bol'shaya Rechka Formation; *7,* early Precambrian complexes of the Sharyzhalgai basement salient of the Siberian craton; *8–11,* intrusive complexes: *8,* Neoproterozoic dolerites; *9,* lamproites; *10,* Paleo–Mesoproterozoic granitoids of the Chernaya Zima (Ignok) complex: *a*, massifs, *b*, large dike bodies; *11*, Paleoproterozoic gabbroids, diorites of the Ust'-Ignok massif; *12,* Paleoproterozoic metadolerites of the Angaul complex; *13,* faults; *14,* bedding; *15,* site of sample 1665.

Zircons were extracted from quartz diorite sample 1665 following a standard heavy-liquid technique. The crystal morphology was examined on a CamScan MX2500S scanning electron microscope in secondary electron and cathodoluminescence modes at the Center for Isotope Research of the Karpinsky Russian Geological Research Institute (CIR VSEGEI), St. Petersburg. A U–Pb geochronological study of zircons was carried out on a SHRIMP-II secondary-ion microprobe at the CIR VSEGEI, following the technique described by Williams (1998). The obtained data were processed using the SQUID software (Ludwig, 2000). The Pb–U ratios were normalized to $^{206}Pb/^{238}U = 0.0668$ in the TEMORA zircon standard, which corresponds to an age of 416.8 Ma (Black et al., 2003). The U and Th contents in the zircons were determined using zircon standard 91500 with a known U content of 81.2 ppm (Wiedenbeck et al., 1995). The ages were estimated with reference to the decay constants for uranium (Steiger and Jäger, 1977). The concordia diagrams were plotted using the ISOPLOT/EX software (Ludwig, 1999). The errors in individual analyses (isotope ratios and ages) and in calculation of the concordant age are at the 1σ and 2σ level, respectively.

RESULTS OF U–Th–Pb GEOCHRONOLOGICAL STUDY

Quartz diorite sample 1665 from the Ust'-Ignok massif was taken near the mouth of the Ignok River (at 53°17.336′N, 100°42.032′E) (Fig. 3). Accessory zircon extracted from the sample occurs as transparent lilac euhedral crystals 100 to 250 μm in size or their fragments. The crystal elongation is 1:2–1:3. The grains show a banded and oscillatory primary magmatic zoning in CL images (Fig. 4*a*). The results of analysis of ten zircon grains are presented in Table 1 and in Fig. 4*b*. These grains have high contents of U (1305–4542 ppm) and Th (981–4034 ppm). The $^{232}Th/^{238}U$ ratio varies from 0.64 to 0.98. In the U–Pb concordia plot (Fig. 4*b*), ten points of the isotope composition of zircon lie on the concordia, and its concordant age is 1836.0 ± 9.7 Ma (MSWD = 0.20). The morphology of zircon is indicative of its magmatic origin, and the date of 1836 ± 10 Ma can be interpreted as the age of zircon crystallization and, accordingly, as the age of diorites of the Ust'-Ignok massif. The obtained data lead to the conclusion that the massif rocks originated at the final stage of the formation of the South Siberian postcollisional magmatic belt.

Table 1. Results of U–Pb analysis of zircons from quartz diorite of the Ust'-Ignok massif (sample 1665)

Sample crystal, crater	$^{206}Pb_c$, %	U ppm	Th ppm	$^{232}Th/^{238}U$	$^{206}Pb^*$, ppm	Isotope ratios								*Rho*	Age, Ma		*D*, %
						$^{238}U/^{206}Pb^*$ (1)	±%	$^{207}Pb^*/^{206}Pb^*$ (1)	±%	$^{207}Pb^*/^{235}U$ (1)	±%	$^{206}Pb^*/^{238}U^*$ (1)	±%		$^{206}Pb/^{238}U$ (1)	$^{207}Pb/^{206}Pb$ (1)	
1665-1.1	0.08	1652	1166	0.73	468	3.034	1.8	0.11200	1.00	5.090	2.1	0.3296	1.8	0.871	1836 ± 29	1832 ± 18	0
1665-2.1	0.10	4542	4034	0.92	1280	3.040	1.7	0.11197	0.63	5.078	1.8	0.3289	1.7	0.939	1833 ± 27	1832 ± 11	0
1665-3.1	0.14	1716	1068	0.64	476	3.103	1.8	0.11190	1.00	4.970	2.1	0.3223	1.8	0.870	1801 ± 28	1830 ± 18	2
1665-4.1	0.08	1305	981	0.78	377	2.978	1.8	0.11160	1.10	5.170	2.1	0.3358	1.8	0.864	1866 ± 30	1825 ± 19	–2
1665-5.1	0.13	1851	1246	0.70	531	2.999	1.8	0.11220	1.20	5.160	2.2	0.3335	1.8	0.831	1855 ± 29	1836 ± 22	–1
1665-6.1	0.10	2276	1553	0.71	639	3.062	1.8	0.11236	0.83	5.059	1.9	0.3265	1.8	0.905	1822 ± 28	1838 ± 15	1
1665-7.1	0.14	3569	2326	0.67	984	3.121	1.8	0.11246	0.74	4.968	1.9	0.3204	1.8	0.921	1791 ± 27	1840 ± 13	3
1665-8.1	0.18	1616	1024	0.65	458	3.036	1.8	0.11270	1.10	5.120	2.2	0.3294	1.8	0.851	1835 ± 29	1844 ± 21	0
1665-9.1	0.12	1571	984	0.65	446	3.029	1.8	0.11400	1.20	5.190	2.2	0.3302	1.8	0.837	1839 ± 29	1864 ± 21	1
1665-10.1	0.00	2091	1990	0.98	598	3.003	1.8	0.11292	0.79	5.180	1.9	0.3330	1.8	0.914	1853 ± 29	1847 ± 14	0

Note. The errors are at the 1σ level. The error in calibration of the standard was 0.57%. Pb_c and Pb* are common and radiogenic lead, respectively. (1) – with common lead correction based on measured ^{204}Pb. Rho is the correlation coefficient of the errors in determination of the $^{206}Pb/^{238}U$ and $^{207}Pb/^{235}U$ ratios, *D* is the discordance.

GEOCHEMISTRY AND ISOTOPE CHARACTERISTICS OF IGNEOUS ROCKS OF THE UST'-IGNOK MASSIF AND THEIR PETROGENESIS

The Ust'-Ignok massif rocks contain 50–63 wt.% SiO_2 and 4.0–6.7 wt.% (Na_2O + K_2O) (Table 2). In the (Na_2O + K_2O)–SiO_2 diagram (Sharpenok et al., 2013), the composition points of the analyzed rocks are arranged along the boundary between normal-alkali and medium-alkali rocks (Fig. 5). The Mg# value of the rocks varies from 53 to 66. Gabbroids–diorites have medium and high contents of TiO_2 (0.63–1.60 wt.%) and P_2O_5 (0.26–0.68 wt.%), which are in good correlation with the SiO_2 contents and Mg#, thus indicating that the rocks belong to the same differentiated series (Fig. 6*a*, *b*). The maximum contents of TiO_2 and P_2O_5 are found in gabbroids.

All igneous rocks of the Ust'-Ignok massif, from gabbro to quartz diorites, show parallel, strongly fractionated REE ($(La/Yb)_n$ = 20–33) and fractionated HREE ($(Gd/Yb)_n$ = 3.4–4.4) patterns (Fig. 7*a*) with a weak or no Eu anomaly (Eu/Eu* = 0.61–0.94) (Fig. 4*a*).

The multielement patterns of the rocks show clear negative Nb–Ta, P, and Ti anomalies. The patterns of gabbroids differ from each other in the Th, U, and Sr region. The other rocks, from gabbrodiorites to quartz diorites, demonstrate parallel patterns (Fig. 7*b*).

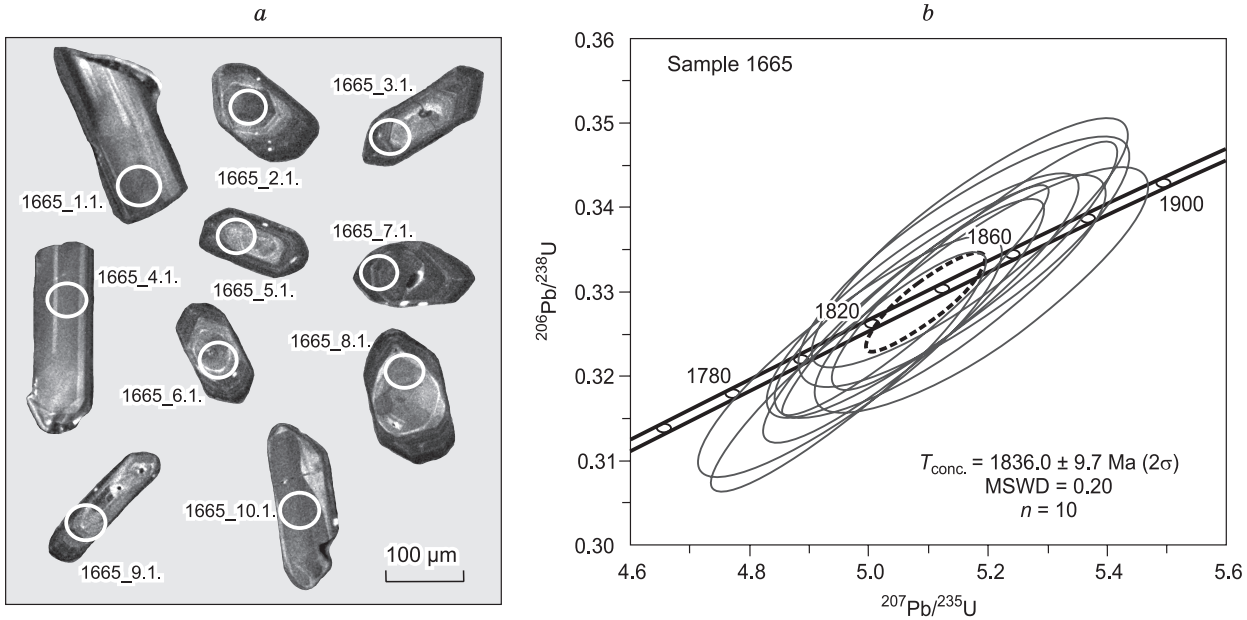

Fig. 4. CL images (*a*) and U–Pb concordia plot (*b*) for zircon crystals from quartz diorite of the Ust'-Ignok massif (sample 1665).

Table 2. Chemical composition of igneous rocks of the Ust'-Ignok massif

Component	1649	1650	1651	1652	1653	1654	1655	1656	1661	1663	1664	1665	1666	1667	1668
SiO_2, wt.%	51.69	55.62	58.66	56.81	58.31	57.58	53.13	53.27	54.52	62.20	62.95	60.58	51.41	49.92	50.04
TiO_2	1.60	0.95	0.82	0.91	0.88	0.84	1.09	1.06	0.94	0.64	0.63	0.73	0.99	1.29	1.21
Al_2O_3	11.73	14.61	15.12	14.56	14.97	14.84	14.15	13.83	13.90	15.05	15.36	15.60	13.04	11.60	11.50
Fe_2O_3	2.45	2.49	2.04	2.25	1.64	1.50	2.22	2.53	3.13	1.09	1.53	1.57	2.15	1.77	2.33
FeO	8.77	5.75	5.28	5.69	5.61	5.77	6.54	6.64	5.98	4.10	3.93	4.54	7.50	8.89	8.19
MnO	0.20	0.17	0.13	0.16	0.12	0.12	0.18	0.17	0.14	0.08	0.09	0.10	0.18	0.20	0.20
MgO	8.00	5.33	3.90	4.76	4.06	4.21	5.94	6.00	5.73	2.94	3.04	3.69	8.30	9.31	9.42
CaO	7.48	6.50	5.16	5.86	4.75	5.41	7.45	7.41	5.46	3.90	3.42	4.90	8.64	10.14	10.42
Na_2O	1.85	2.82	3.01	2.70	2.90	3.17	3.15	3.46	3.16	4.00	3.94	3.83	2.15	2.08	2.12
K_2O	2.18	3.08	3.34	3.24	3.32	3.03	2.99	2.36	1.83	2.58	2.73	2.07	2.52	2.16	2.37
P_2O_5	0.68	0.49	0.39	0.46	0.40	0.41	0.55	0.49	0.52	0.27	0.26	0.31	0.58	0.62	0.61
LOI	3.00	1.98	1.84	2.20	2.47	2.23	2.10	2.04	3.13	2.05	1.92	1.81	2.06	1.86	1.20
H_2O^-	0.07	0.04	0.06	0.09	0.00	0.06	0.06	0.08	0.06	0.06	0.04	0.00	0.08	0.09	0.08
CO_2	0.64	0.10	0.00	0.00	0.44	0.54	0.31	0.25	1.31	0.59	0.19	0.00	0.00	0.09	0.21
Total	100.35	99.92	99.75	99.69	99.88	99.70	99.86	99.59	99.81	99.55	100.02	99.74	99.59	100.01	99.90
Rb, ppm	73	83	100	92	108	90	69	57	49	61	56	47	97	92	87
Sr	440	761	689	637	577	593	608	620	600	627	641	838	848	680	759
Y	38	25	22	26	20	23	27	27	24	17	17	19	26	30	30
Zr	125	191	238	205	189	219	231	223	179	215	213	229	132	139	73
Nb	12	10	9	11	10	10	12	10	10	9	10	9	8	8	8
Ba	865	1123	1027	962	1184	1084	997	815	833	760	747	868	1031	880	1130
La	111.51	69.80	63.45	82.06	64.20	72.44	77.24	73.19	81.11	66.06	64.68	52.48	74.62	69.73	65.91
Ce	203.44	156.02	136.19	176.47	132.20	161.30	168.61	158.38	160.38	122.20	121.92	116.46	149.71	149.44	143.93
Pr	23.53	17.41	15.12	19.08	14.33	17.36	19.04	18.34	19.04	13.43	13.27	12.85	18.59	19.16	18.59
Nd	91.06	65.28	56.59	69.33	52.41	59.80	70.49	68.78	71.07	47.96	47.44	47.54	71.01	75.57	75.68
Sm	18.53	12.69	11.05	13.28	9.49	10.52	13.56	13.33	12.97	8.05	8.01	8.79	13.84	14.72	15.10
Eu	3.05	2.65	2.39	2.65	2.17	2.23	2.90	3.05	3.07	2.11	2.05	2.28	3.28	3.44	3.48
Gd	12.77	8.75	7.34	9.01	6.95	7.43	9.29	9.88	9.21	5.98	5.92	6.54	9.95	11.27	10.88
Tb	1.65	1.07	0.95	1.15	0.86	0.97	1.25	1.26	1.20	0.80	0.77	0.84	1.31	1.49	1.55
Dy	7.80	5.35	4.55	5.30	4.16	4.59	5.66	5.68	5.77	3.86	3.63	4.17	6.28	7.28	7.26
Ho	1.38	0.89	0.78	0.88	0.70	0.80	0.97	0.98	0.96	0.67	0.62	0.72	1.04	1.19	1.17
Er	3.37	2.14	1.85	2.28	1.72	1.99	2.33	2.38	2.28	1.70	1.53	1.72	2.45	2.71	2.69
Tm	0.45	0.29	0.26	0.31	0.24	0.31	0.32	0.34	0.32	0.23	0.21	0.24	0.34	0.37	0.36
Yb	2.58	1.93	1.58	1.92	1.43	1.87	1.92	1.98	1.88	1.41	1.26	1.42	2.05	2.18	2.15
Lu	0.40	0.27	0.25	0.29	0.23	0.32	0.28	0.29	0.25	0.21	0.18	0.21	0.31	0.32	0.33
Hf	3.41	5.03	5.76	5.33	4.73	5.80	5.35	5.46	4.29	5.04	4.94	5.44	3.26	3.36	2.22
Ta	0.68	0.59	0.48	0.70	0.68	0.79	0.63	0.62	0.56	0.45	0.58	0.53	0.25	0.17	0.38
Th	14.46	12.23	13.22	21.51	9.77	9.43	12.93	15.79	14.83	15.18	15.65	11.12	7.66	3.27	2.72
U	2.23	2.30	1.75	2.49	2.33	2.37	3.23	3.62	2.73	2.62	2.88	1.76	1.77	0.81	0.69
Mg#	60	58	53	56	55	55	59	59	58	55	55	56	65	65	66
$(La/Yb)_n$	28.0	23.4	25.9	27.7	29.1	25.0	26.0	23.9	27.9	30.4	33.3	23.9	23.6	20.7	19.8
Eu/Eu*	0.61	0.77	0.82	0.75	0.82	0.78	0.80	0.82	0.87	0.94	0.92	0.93	0.86	0.82	0.84
$(Gd/Yb)_n$	4.2	3.8	3.9	4.0	4.1	3.4	4.1	4.2	4.1	3.6	4.0	3.9	4.1	4.4	4.3
Nb/Nb*	0.10	0.11	0.11	0.09	0.13	0.13	0.12	0.10	0.10	0.10	0.10	0.13	0.11	0.17	0.19
Ti/Ti*	0.24	0.21	0.22	0.20	0.25	0.22	0.23	0.22	0.20	0.22	0.21	0.23	0.20	0.23	0.22
$(Th/La)_{PM}$	1.05	1.42	1.68	2.12	1.23	1.05	1.35	1.74	1.48	1.86	1.96	1.71	0.83	0.38	0.33
$(Nb/La)_{PM}$	0.11	0.13	0.14	0.13	0.14	0.14	0.14	0.13	0.12	0.13	0.14	0.17	0.10	0.11	0.11
La/Nb	9.0	7.3	6.9	7.5	6.7	7.1	6.7	7.5	8.3	7.4	6.7	5.6	9.8	9.0	8.8
La/Ta	163	118	132	117	94	91	123	118	145	145	111	100	296	422	171

Note. Mg# = Mg·100/(Mg + Fe^{2+}), where Mg = MgO/40.31, Fe^{2+} = ($Fe_2O_3^*$ × 0.8998 × 0.85)/71.85; Eu/Eu* = $Eu_n/\left(\sqrt{Sm_n \times Gd_n}\right)$, Nb/Nb* = $Nb_{PM}/\left(\sqrt{Th_{PM} \times La_{PM}}\right)$, Ti/Ti* = $Ti_{PM}/\left(\sqrt{Sm_{PM} \times Gd_{PM}}\right)$; *n*, chondrite-normalized (Wakita et al., 1970), PM, primitive-mantle-normalized (Sun and McDonough, 1989).

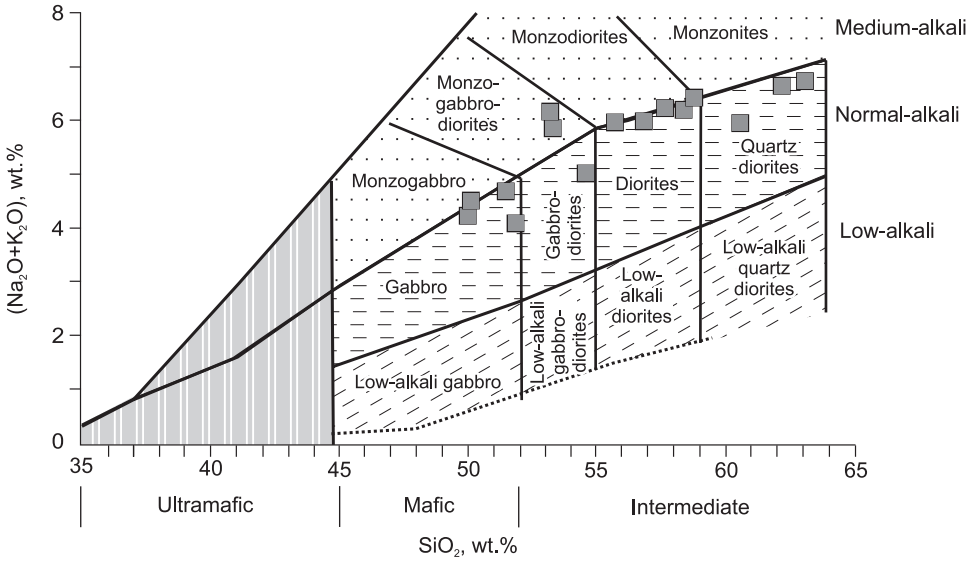

Fig. 5. ($Na_2O + K_2O$)–SiO_2 diagram (Sharpenok et al., 2008) for rocks of the Ust'-Ignok massif.

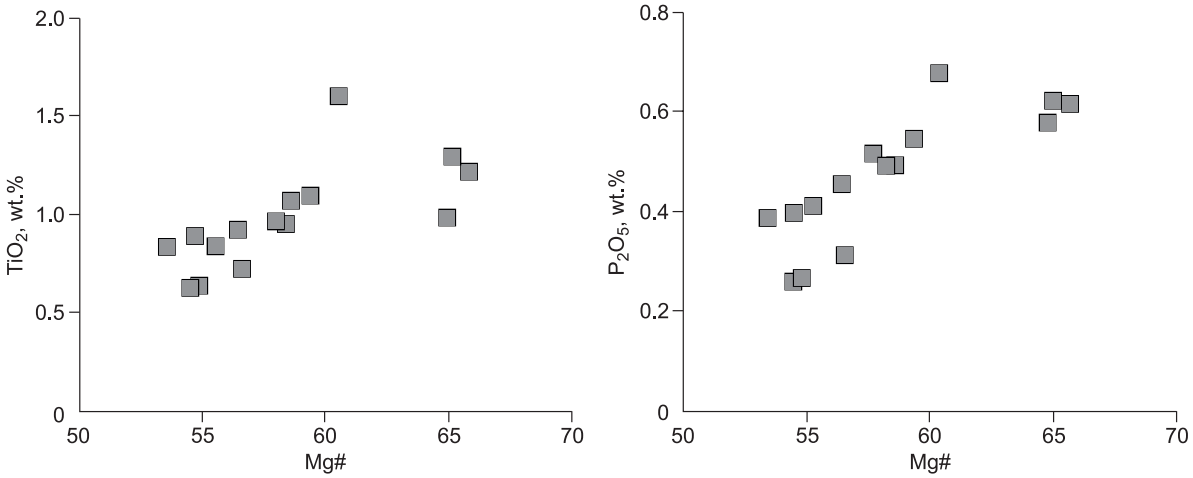

Fig. 6. Mg#–TiO_2 and Mg#–P_2O_5 variation diagrams for the Ust'-Ignok massif rocks.

The analyzed igneous rocks are characterized by $\varepsilon_{Nd}(T)$ from +0.3 to –0.9 and by a early Proterozoic Nd model age $T_{Nd}(DM)$ = 2.3–2.4 Ga (Fig. 8; Table 3).

As mentioned above, all igneous rocks of the Ust'-Ignok massif demonstrate clear negative Nb–Ta and Ti anomalies in the multielement patterns (Fig. 7*b*). In addition, their composition points lie beyond the N-MORB–E-MORB–OIB field in the Th/Yb–Nb/Yb diagram (Pearce, 2008) and fall in the field of rocks of mantle origin either containing a subductional component or contaminated with crustal material (Fig. 9*a*). The massif gabbro have high contents of K_2O (2.16–2.52 wt.%) and P_2O_5 (0.58–0.68 wt.%), close to those in OIB, but medium contents of TiO_2 (0.99–1.60 wt.%), Nb (8–12 ppm), and Th (2.7–14.5 ppm) and high contents of Sr (440–848 ppm), Ba (865–1130 ppm), and La (66–112 ppm), typical of suprasubductional basalts. In addition, they are characterized by $(Th/La)_{PM}$ = 0.33–1.05 (i.e., ≤1), which indicates insignificant contamination of their source with con-

Table 3. Sm–Nd isotope data for igneous rocks of the Ust'-Ignok massif

Sample	Rock	Age, Ma	Content, ppm		$^{147}Sm/^{144}Nd$	$^{143}Nd/^{144}Nd$ ±2σ	$\varepsilon_{Nd}(T)$	$T_{Nd}(DM)$	$T_{Nd}(DM\text{-}2st)$
			Sm	Nd				Ma	
1651	Diorite	1836	7.18	32.50	0.1193	0.511716 ± 10	0.3	2309	2313
1665	Quartz diorite	1836	5.31	23.60	0.1215	0.511685 ± 10	–0.9	2415	2405
1668	Gabbro	1836	10.73	45.01	0.1286	0.511797 ± 16	–0.4	2416	2363

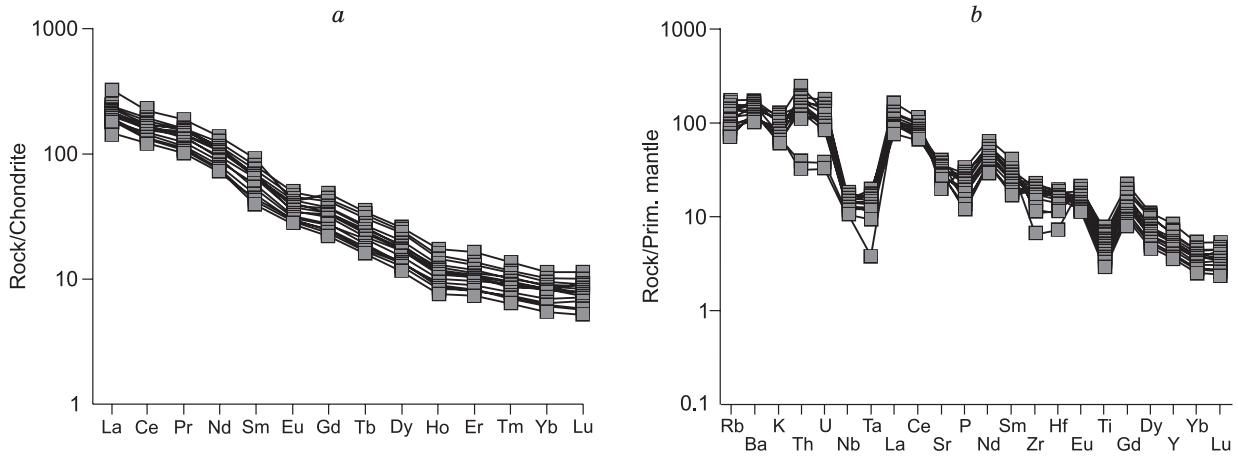

Fig. 7. Chondrite-normalized (Wakita et al., 1970) REE patterns (*a*) and primitive-mantle-normalized (Sun and McDonough, 1989) multielement patterns (*b*) for the Ust'-Ignok massif rocks.

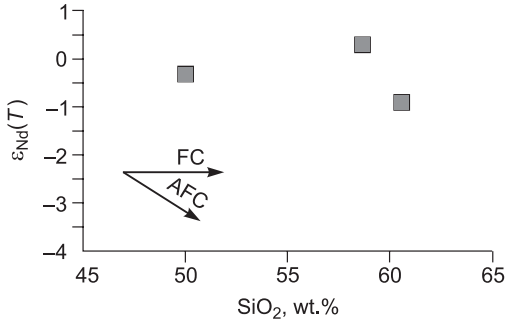

Fig. 8. $\varepsilon_{Nd}(T)$–SiO_2 diagram for the Ust'-Ignok massif rocks. FC, fractional crystallization, AFC, assimilation–fractional crystallization.

tinental-crust material (Fig. 9*b*). The massif rocks formed in a postcollisional-extension setting after the end of all subduction and collision events in the region (Gladkochub et al., 2006). Therefore, the geochemical parameters of the gabbroids reflect the composition of the melted mantle source rather than the geodynamic setting of their formation. The geochemical parameters of the massif gabbro and their high indicator ratios La/Nb = 8.8–9.8 and La/Ta = 163–422 (Table 2) suggest their formation through the melting of an enriched lithospheric-mantle source with suprasubductional geochemical characteristics. The more felsic massif rocks, from gabbrodiorites to quartz diorites, apparently resulted from the fractional crystallization of gabbroids. The Ust'-Ignok massif rocks are characterized by $\varepsilon_{Nd}(T)$ values from –0.9 to +0.3 showing no correlation with the SiO_2 contents and thus confirming the formation of the more felsic rocks as a result of fractional crystallization rather than the addition of crustal material to the mantle source (Fig. 8). The good correlation between Mg# and CaO/Al_2O_3 (r = 0.95) suggests clinopyroxene as one of major fractionating phases, which is confirmed by petrographic studies.

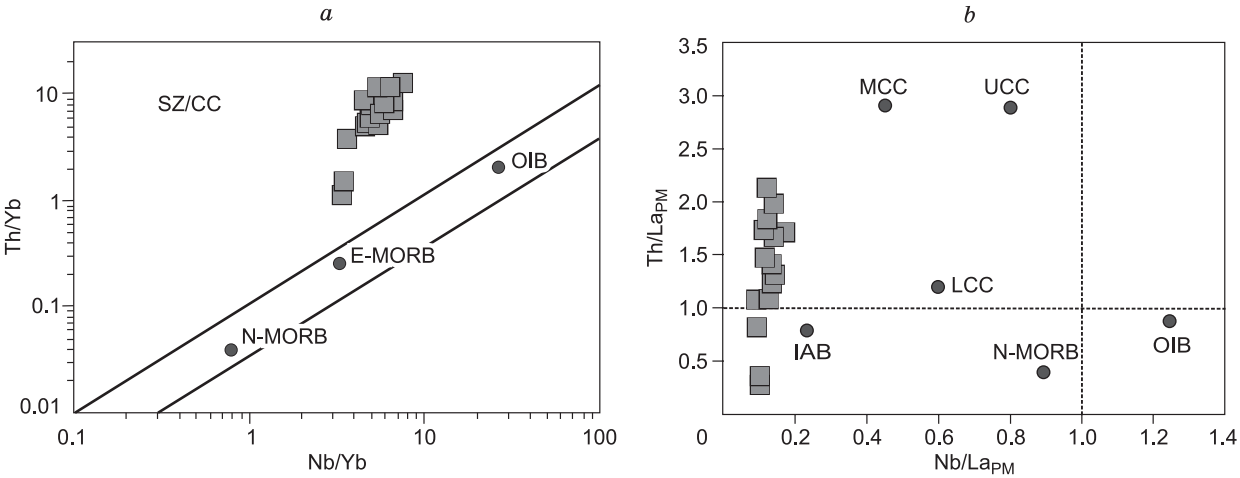

Fig. 9. Th/Yb–Nb/Yb (Pearce, 2008) (*a*) and $(Th/La)_{PM}$–$(Nb/La)_{PM}$ (Donskaya et al., 2014) (*b*) diagrams for the Ust'-Ignok massif rocks. IAB, island arc basalts, N-MORB and E-MORB, normal (N) and enriched (E) mid-ocean ridge basalts, OIB, oceanic-island basalts, UCC, upper continental crust, MCC, middle continental crust, LCC, lower continental crust, SZ/CC, zone of rocks of mantle origin or rocks containing a subductional component or contaminated with crustal material.

DISCUSSION

Mafic igneous rocks are found throughout the area of outcropping rocks of the South Siberian postcollisional magmatic belt: from the Biryusa basement salient in the west to the Aldan Shield in the east (Fig. 1; Table 4). They are subordinate relative to granitoids and felsic volcanics. Mafic rocks intruded over the entire period of formation of the South Siberian magmatic belt, 1.88–1.84 Ga (Table 4). Note that the age of some mafic rocks was determined by U–Pb zircon and baddeleyite dating, and the age of others was taken similar to the age of the associated felsic rocks (Table 4). Mafic-magmatism intrusions and associations of mafic and other igneous rocks are diverse within the belt: (1) dolerite and gabbrodolerite dikes (Kuranakh and Kalar–Nimnyr complexes of the Aldan Shield) (Okrugin et al., 1995; Popov et al., 2012; Ernst et al., 2016); (2) lamprophyre dikes (Sharyzhalgai salient) (Ivanov et al., 2019); (3) composite dolerite–granite/rhyolite dikes (Sharyzhalgai salient, North Baikal volcanoplutonic belt of the Baikal salient) (Shokhonova et al., 2010; Gladkochub et al., 2013), (4) dolerite dikes and associated volcanics of mafic and intermediate composition (Mal'tsev Formation, Sayan–Biryusa volcanoplutonic belt, Biryusa salient) (Donskaya et al., 2019); (5) basalts and basaltic andesites of volcanoterrigenous stratified formations (lower part of the Akitkan Group, North Baikal volcanoplutonic belt of the Baikal salient) (Neimark et al., 1998; Shokhonova et al., 2010); (6) gabbroid massifs in association with ultramafic rocks and anorthosites (Malyi Zadoi massif of the Sharyzhalgai salient, massifs of the Chinei complex of the Aldan Shield) (Gongalsky et al., 2008a,b; Popov et al., 2009; Gongalsky, 2010; Mekhonoshin et al., 2016); (7) gabbroid massifs in association with diorites (Ust'-Ignok massif of the Urik–Iya graben) (this paper). Such a variety of mafic-magmatism intrusions and associations is apparently typical of a postcollisional-extension setting, when different scenarios of mafic magmatism are possible.

Mafic rocks (1.88–1.84 Ga) of the South Siberian postcollisional magmatic belt show both similar and different geochemical features. Most of them are normal- and medium-alkali rocks (Fig. 10*a*). Gabbronorites of the Malyi Zadoi massif of the Sharyzhalgai salient are the only low-alkali rocks. Almost all composition points of these mafic rocks lie beyond the N-MORB–E-MORB–OIB field in the Th/Yb–Nb/Yb diagram (Pearce, 2008) and fall in the field of rocks of mantle origin or rocks containing a subductional component or contaminated with crustal material (Fig. 10*b*). All the rocks show a variably expressed negative Nb anomaly in the multielement patterns ($Nb/Nb^* < 1$). Their $(Th/La)_{PM}$ value can be both <1 and >1, even within the same massif or dike swarm (Fig. 10*c*). This fact rejects the crustal-material

Table 4. Characteristics of mafic igneous rocks of the South Siberian postcollisional magmatic belt

Siberian craton terrane	Complex/formation/ massif	General characteristics of igneous rocks	Characteristics of mafic rocks	Age, Ma	Dated rock, method, material	Reference
Biryusa salient	Sayan–Biryusa volcanoplutonic belt, Mal'tsev Formation of the Elash Group	Volcanics of different compositions, subvolcanic rocks	Dolerites, gabbrodolerites, basaltic andesites	1872 ± 10 1874 ± 10	Felsic volcanics, U–Pb (SHRIMP), zircon	(Donskaya et al., 2019)
Urik–Iya graben	Ust'-Ignok massif	Gabbroids, diorites	Gabbro, gabbrodiorites	1836 ± 10	Quartz diorite, U–Pb (SHRIMP), zircon	(This work)
Sharyzhalgai salient	Composite dikes in the Kitoi River area	Gabbrodolerites, granites	Gabbrodolerites	1864.3 ± 4.2	Gabbrodolerite, U–Pb (TIMS), zircon	(Gladkochub et al., 2013)
	Malyi Zadoi massif	Plagioperidotites, gabbronorites, anorthosites	Gabbronorites	1863 ± 1	Gabbronorite, U-Pb (TIMS), baddeleyite	(Mekhonoshin et al., 2016; Ernst et al., 2016)
	Small unnamed massifs in the Kitoi River area	Dolerites, lamprophyres	Dolerites, lamprophyres	1864.7 ± 1.8	Lamprophyre, U–Pb (TIMS), zircon	(Ivanov et al., 2019)
Baikal salient	Sayan–Biryusa volcanoplutonic belt, lower Akitkan Group	Basalts, basaltic andesites, dacites, rhyolites	Basalts, basaltic andesites	1877.7 ± 3.8	Dacite, U–Pb (TIMS), zircon	(Donskaya et al., 2008)
	Sayan–Biryusa volcanoplutonic belt, composite dikes and dolerite dikes in the Svetlyi Brook area	Dolerites, rhyolites	Dolerites	1844 ± 11	Rhyolite, U–Pb (SHRIMP), zircon	(Shokhonova et al., 2010)
Aldan Shield	Chinei complex, massifs, and dikes	Pyroxenites, gabbronorites, gabbro, anorthosites	Gabbronorites, gabbro	1867 ± 3	Gabbrodiorite, U–Pb (TIMS), zircon	(Popov et al., 2009)
	Kuranakh complex, dikes	Dolerites, gabbrodolerites	Dolerites, gabbrodolerites	1867 ± 9	Dolerite, U–Pb (TIMS), zircon	(Popov et al., 2012)
	Kalar–Nimnyr complex, dikes	Dolerites	Dolerites	1869 ± 2	Dolerite, U-Pb (TIMS), baddeleyite	(Ernst et al., 2016)

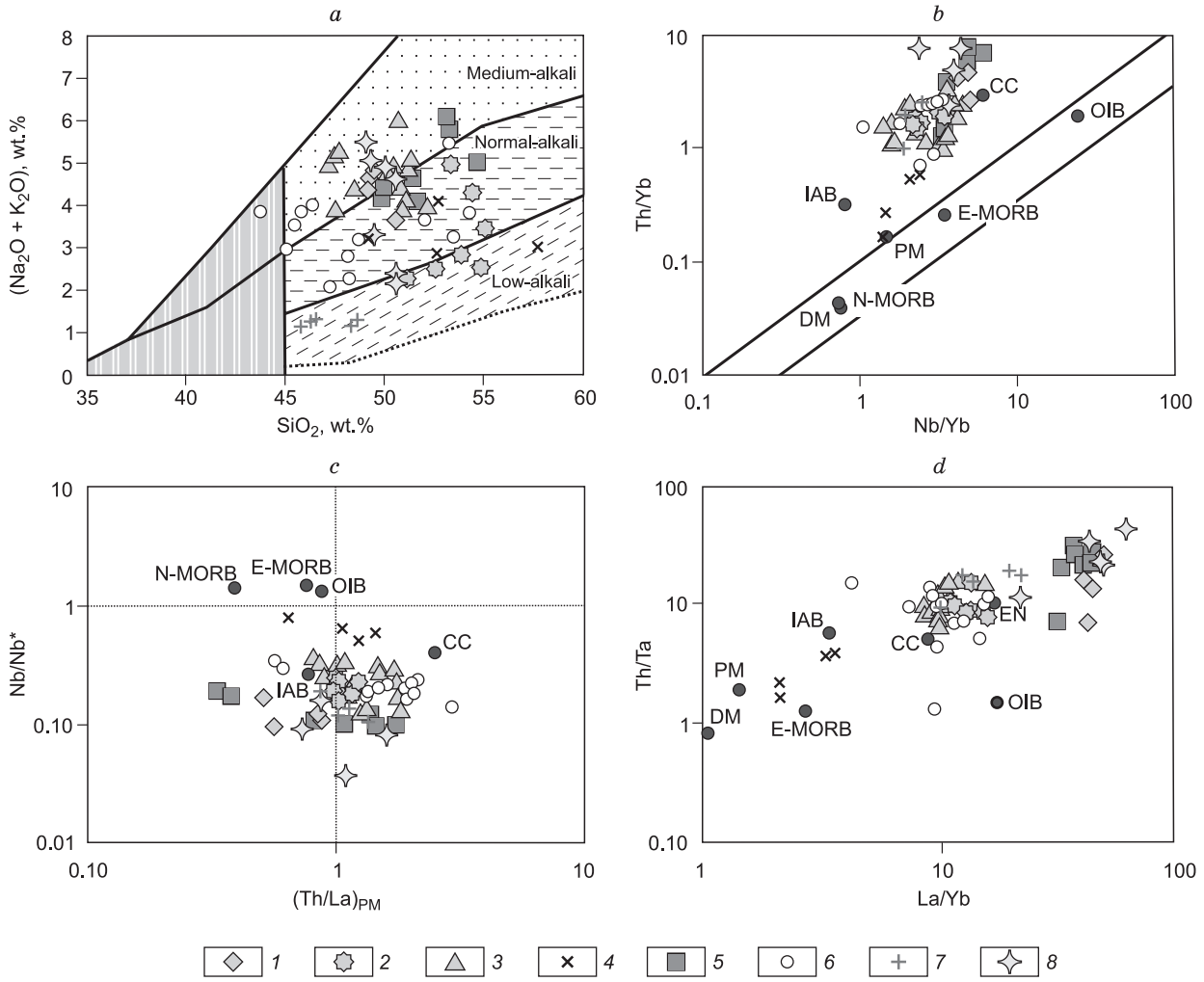

Fig. 10. ($Na_2O + K_2O$)–SiO_2 (Sharpenok et al., 2008) (*a*), Th/Yb–Nb/Yb (Pearce, 2008) (*b*), Nb/Nb*–$(Th/La)_{PM}$ (*c*), and Th/Ta–La/Yb (Condie, 1997) (*d*) diagrams for early Proterozoic mafic rocks of the South Siberian postcollisional magmatic belt. Chemical compositions are given in Table 2 and in earlier publications (Gongalsky, 2008a; Shokhonova et al., 2010; Gladkochub et al., 2013; Mekhonoshin et al., 2016; Donskaya et al., 2019; Ivanov et al., 2019; our and Mekhonoshin's unpublished data). IAB, island arc basalts, N-MORB and E-MORB, normal (N) and enriched (E) mid-ocean ridge basalts, OIB, oceanic-island basalts, CC, continental crust, DM, depleted mantle, PM, primitive mantle, EN, enriched component. *1,* composite-dike dolerites of the Sharyzhalgai salient (Gladkochub et al., 2013); *2*, lower Akitkan Group basaltoids of the North Baikal volcanoplutonic belt of the Baikal salient (Shokhonova et al., 2010); *3*, composite-dike dolerites of the North Baikal volcanoplutonic belt of the Baikal salient (Shokhonova et al., 2010); *4*, Mal'tsev Formation dolerites and basaltoids of the Sayan–Biryusa volcanoplutonic belt of the Biryusa salient (Donskaya et al., 2019); *5*, gabbro and gabbrodiorites of the Ust'-Ignok massif of the Urik-Iya graben (this paper); *6*, gabbroids of the Chinei complex of the Aldan Shield (Gongalsky et al., 2008a, 2016; Gongalskiy, 2010); *7*, gabbroids of the Malyi Zadoi massif of the Sharyzhalgai salient (Mekhonoshin et al., 2016; Mekhonoshin's unpublished data); *8*, lamprophyre dikes of the Sharyzhalgai salient (Ivanov et al., 2019).

contamination of mantle sources for all studied rocks, because continental-crust rocks always show $(Th/La)_{PM} > 1$ (Fig. 10*c*) and, thus, basaltic melts contaminated with crustal material are also characterized by $(Th/La)_{PM} > 1$. This is their difference from noncontaminated rocks, including suprasubductional basalts with a varying $(Th/La)_{PM}$ value. In the Th/Ta–La/Yb diagram (Condie, 1997), most of the composition points of the considered mafic rocks, except for volcanics of the Mal'tsev Formation of the Sayan–Biryusa volcanoplutonic belt, are arranged around the point of enriched component (EN) (Fig. 10*d*). In addition, all these rocks have La/Nb > 2.5 and negative or near-zero $\varepsilon_{Nd}(T)$ values (Fig. 11). The above geochemical features altogether suggest that most of the mafic igneous rocks of the South Siberian postcollisional magmatic belt resulted from the melting of the subcontinental lithospheric mantle with suprasubductional geochemical characteristics, which, in turn, might have formed during subduction processes preceding the formation of the Siberian craton. Note that some mafic rocks might have originated from multicomponent mantle sources rather than from the simple melting of the lithospheric mantle. For example, the hard-melting lithospheric mantle metasomatized by subductional fluids was assumed to be a source for dike dolerites of the North Baikal volca-

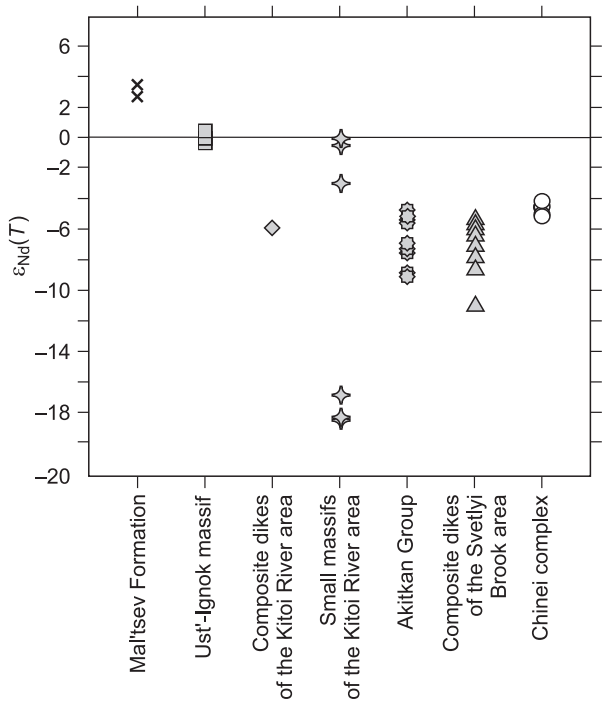

Fig. 11. $\varepsilon_{Nd}(T)$ values of mafic igneous rocks of the South Siberian postcollisional magmatic belt. The Nd isotope composition is given in Table 3 and in the earlier publications (Gongalsky et al., 2008b; Shokhonova et al., 2010; Donskaya et al., 2019; Ivanov et al., 2019; our unpublished data).

noplutonic belt (Shokhonova et al., 2010), and highly metasomatized lithosphere mantle was considered to form lamprophyres of the Sharyzhalgai salient (Ivanov et., 2019). Turkina and Kapitonov (2019) believe that the enriched subcontinental lithospheric mantle was generated during the Neoarchean subduction. At the same time, Shokhonova et al. (2010) and Ivanov et al. (2019) concluded that this mantle formed in the course of early Proterozoic subductional processes. Let us leave aside the time of the subduction events contributing to the formation of the enriched subcontinental lithosphere beneath the southern Siberian craton, which was the source of material for mafic igneous rocks of the South Siberian postcollisional magmatic belt. If we treat these rocks as potential suppliers of mantle material for granitoids and felsic volcanics of similar age, we should bear in mind that most of them have suprasubductional characteristics and negative $\varepsilon_{Nd}(T)$ values.

It is admitted that dolerites and andesitic basalts of the Mal'tsev Formation of the Sayan–Biryusa volcanoplutonic belt might have formed from a mantle source other than the enriched subcontinental lithospheric mantle, namely, the source that resulted from mixing of a depleted component of the asthenospheric mantle and, probably, a plume component, without a significant contribution of the lithospheric mantle (Donskaya et al., 2019). The composition points of the Mal'tsev Formation lie near the points of mantle rocks in the discrimination diagrams (Fig. 10) and are characterized by La/Nb = 1.4–1.7 (Donskaya et al., 2019). In addition, the Mal'tsev Formation rocks are the only ones of all mafic rocks of the South Siberian belt that show high positive $\varepsilon_{Nd}(T)$ values, +3.7 and +4.1 (Donskaya et al., 2019). Note, however, that the fractional content of the Mal'tsev Formation rocks is very small within the South Siberian belt. Therefore, they can hardly be treated as potential sources of mantle material throughout the area of outcropping granitoids and felsic volcanics of the South Siberian postcollisional magmatic belt.

CONCLUSIONS

(1) The Ust'-Ignok gabbrodiorite massif of the Urik–Iya graben of the Siberian craton is composed of igneous rocks of the continuous series from biotite gabbro via gabbrodiorites and diorites to quartz diorites.

(2) The U–Pb zircon dating of quartz diorite of the Ust'-Ignok massif yielded an age of 1836 ± 10 Ma, i.e., the massif rocks might have originated at the final stage of the formation of the South Siberian postcollisional magmatic belt (which formed in the period 1.88–1.84 Ga).

(3) The rocks of the Ust'-Ignok massif are normal and medium alkalinity. All igneous rocks from gabbro to quartz diorites show highly fractionated REE patterns ($(La/Yb)_n$ = 20–33) and clear negative anomalies of Nb–Ta and Ti in their multielement patterns; their $\varepsilon_{Nd}(T)$ values vary from +0.3 to –0.9. The geochemical indicator ratios in the gabbroids point to insignificant contamination of their source with continental-crust material and to their formation through the melting of an enriched lithospheric-mantle source. Gabbrodiorites–quartz diorites of the Ust'-Ignok massif resulted, most likely, from the fractional crystallization of gabbroids.

(4) Mafic-magmatism intrusions and associations are diverse and widespread within the South Siberian postcollisional magmatic belt. These are dolerite and lamprophyre dikes, composite dikes, massifs composed of rocks of ultramafic, mafic, and intermediate compositions, and volcanics. Such diversity is typical of a postcollisional-extension setting.

(5) Analysis of the geochemical and isotope characteristics of mafic igneous rocks of the South Siberian postcollisional magmatic belt has shown that most of them resulted from the melting of an enriched lithospheric mantle source with a subductional component. This source might have formed during the subduction processes preceding the formation of the Siberian craton. Thus, if the mafic rocks are treated as potential sources of mantle material for nearly coeval granitoids and felsic volcanics, the latter will inevitably have their specific suprasubductional characteristics.

The geological, geochemical, and isotope-geochemical studies were supported by grant 18-17-00101 from the Russian Science Foundation, and the geochronological studies, by grant 18-05-00764 from the Russian Foundation for Basic Research.

REFERENCES

Black, L.P., Kamo, S.L., Allen, C.M., Aleinikoff, J.N., Davis, D.W., Korsch, R.J., Foudoulis, C., 2003. TEMORA 1: a new zircon standard for Phanerozoic U–Pb geochronology. Chem. Geol. 200 (1–2), 155–170.

Condie, K.C., 1997. Sources of Proterozoic mafic dyke swarms: constraints from Th/Ta and La/Yb ratios. Precambrian Res. 81 (1–2), 3–14.

Didenko, A.N., Vodovozov, V.Yu., Pisarevsky, S.A., Gladkochub, D.P., Donskaya, T.V., Mazukabzov, A.M., Stanevich, A.M., Bibikova, E.V., Kirnozova, T.I., 2009. Palaeomagnetism and U–Pb dates of the Palaeoproterozoic Akitkan Group (South Siberia) and implications for pre-Neoproterozoic tectonics, in: Reddy, S.M., Mazumber, R., Evans, D.A.D., Collins, A.S. (Eds.), Palaeoproterozoic Supercontinents and Global Evolution. Geol. Soc. London Spec. Publ. Vol. 323, pp. 145–163.

Donskaya, T.V., Gladkochub, D.P., Kovach, V.P., Mazukabzov, A.M., 2005. Petrogenesis of early Proterozoic postcollisional granitoids in the southern Siberian craton. Petrology 13 (3), 229–252.

Donskaya, T.V., Bibikova, E.V., Gladkochub, D.P., Mazukabzov, A.M., Bayanova, T.B., De Waele, B., Didenko, A.N., Bukharov, A.A., Kirnozova, T.I., 2008. Petrogenesis and age of the felsic volcanic rocks from the North Baikal volcanoplutonic belt, Siberian craton. Petrology 16 (5), 422–447.

Donskaya, T.V., Gladkochub, D.P., Mazukabzov, A.M., Wingate, M.T.D., 2014. Early Proterozoic postcollisional granitoids in the Biryusa block of the Siberian craton. Russian Geology and Geophysics (Geologiya i Geofizika) 55 (7), 812–823 (1028–1043).

Donskaya, T.V., Gladkochub, D.P., Mazukabzov, A.M., Denyszyn, S., Pisarevsky, S.A., Motova, Z.L., Demonterova, E.I., 2018. The oldest (~1.9 Ga) metadolerites of the southern Siberian craton: age, petrogenesis, and tectonic setting. Russian Geology and Geophysics (Geologiya i Geofizika) 59 (12), 1548–1559 (1941–1957).

Donskaya, T.V., Gladkochub, D.P., Mazukabzov, A.M., L'vov, P.A., Demonterova, E.I., Motova, Z.L., 2019. Sayan–Biryusa volcanoplutonic belt (southern Siberian craton): age and petrogenesis. Russian Geology and Geophysics (Geologiya i Geofizika) 60 (1), 14–32 (18–40).

Ernst, R.E., Hamilton, M.A., Söderlund, U., Hanes, J.A., Gladkochub, D.P., Okrugin, A.V., Kolotilina, T., Mekhonoshin, A.S., Bleeker, W., LeCheminant, A.N., Buchan, K.L., Chamberlain, K.R., Didenko, A.N., 2016. Long-lived connection between southern Siberia and northern Laurentia in the Proterozoic. Nat. Geosci. 9 (6), 464–469.

Galimova, T.F., Pashkova, A.G., Povarintseva, S.A., Perfil'ev, V.V., Namolova, M.M., Andryushchenko, S.V., Denisenko, E.P., Permyakov, S.A., Mironyuk, E.P., Timashkov, A.N., Plekhanov, A.O., 2012. State Geological Map of the Russian Federation, Scale 1 : 1,000,000 (Third Edition). Angara–Yenisei Series. Sheet N-47: Nizhneudinsk. Explanatory Note [in Russian]. Kartograficheskaya Fabrika VSEGEI, St. Petersburg.

Gladkochub, D.P., Pisarevsky, S.A., Donskaya, T.V., Natapov, L.M., Mazukabzov, A.M., Stanevich, A.M., Sklyarov, E.V., 2006. Siberian Craton and its evolution in terms of Rodinia hypothesis. Episodes 29 (3), 169–174.

Gladkochub, D.P., Pisarevsky, S.A., Donskaya, T.V., Ernst, R.E., Wingate, M.T.D., Söderlund, U., Mazukabzov, A.M., Sklyarov, E.V., Hamilton, M.A., Hanes, J.A., 2010. Proterozoic mafic magmatism in Siberian craton: An overview and implications for paleocontinental reconstruction. Precambrian Res. 183 (3), 660–668.

Gladkochub, D.P., Donskaya, T.V., Ernst, T., Mazukabzov, A.M., Sklyarov, E.V., Pisarevsky, S.A., Wingate, M., Söderlund, U., 2012. Proterozoic basic magmatism of the Siberian craton: main stages and their geodynamic interpretation. Geotectonics 46 (4), 273–284.

Gladkochub, D.P., Pisarevsky, S.A., Mazukabzov, A.M., Söderlund, U., Sklyarov, E.V., Donskaya, T.V., Ernst, T., Stanevich, A.M., 2013. The first evidence of Paleoproterozoic late-collision basite magmatism in the near-Sayan salient of the Siberian craton basement. Dokl. Earth Sci. 450 (2), 583–586.

Gladkochub, D.P., Mazukabzov, A.M., Stanevich, A.M., Donskaya, T.V., Motova, Z.L., Vanin, V.A., 2014. Precambrian sedimentation in the Urik–Iya graben, southern Siberian craton: main stages and tectonic settings. Geotectonics 48 (5), 359–370.

Goldstein, S.J., Jacobsen, S.B., 1988. Nd and Sr isotopic systematics of river water suspended material: implications for crustal evolution. Earth Planet. Sci. Lett. 87 (3), 249–265.

Gongalskiy, B.I., 2010. Specific features of the basic magmatism in the Udokan–Chineyskiy region (Northern Transbaikalia). Litosfera, No. 3, 87–94.

Gongalsky, B.I., Krivolutskaya, N.A., Ariskin, A.A., Nikolaev, G.S., 2008a. Inner structure, composition, and genesis of the Chineiskii anorthosite–gabbronorite massif, Northern Transbaikalia. Geochem. Int. 46 (7), 637–665.

Gongalsky, B.I., Sukhanov, M.K., Gol'tsman, Yu.V., 2008b. The Sm–Nd Isotope System of the Chinei Anorthosite–Gabbronorite Massif (Eastern Transbaikalia). Problems of Geology of Ore Deposits, Mineralogy, Petrology, and Geochemistry [in Russian]. IGEM RAN, Moscow, pp. 57–60.

Gongalsky, B.I., Krivolutskaya, N.A., Ariskin, A.A., Nikolaev, G.S., 2016. The Chineysky gabbronorite–anorthosite layered massif (Northern Transbaikalia, Russia): its structure, Fe–Ti–V and Cu–PGE deposits, and parental magma composition. Mineral. Deposita 51 (8), 1013–1034.

Ivanov, A.V., Levitskii, I.V., Levitskii, V.I., Corfu, F., Demonterova, E.I., Reznitskii, L.Z., Pavlova, L.A., Kamenetsky, V.S., Savatenkov, V.M., Powerman, V.I., 2019. Shoshonitic magmatism in the Paleoproterozoic of the south-western Siberian Craton: An analogue of the modern post-collision setting. Lithos 328–329, 88–100.

Jacobsen, S.B., Wasserburg, G.J., 1984. Sm–Nd isotopic evolution of chondrites and achondrites, II. Earth Planet. Sci. Lett. 67 (2), 137–150.

Larin, A.M., Sal'nikova, E.B., Kotov, A.B., Kovalenko, V.I., Rytsk, E. Yu., Yakovleva, S.Z., Berezhnaya, N.G., Kovach, V.P., Buldygerov, V.V., Sryvtsev, N.A., 2003. The North Baikal volcanoplutonic belt: age, formation duration, and tectonic setting. Dokl. Earth Sci. 392 (7), 963–967.

Ludwig, K.R., 1999. User's Manual for Isoplot/Ex, Version 2.10. A Geochronological Toolkit for Microsoft Excel. Berkeley Geochronology Center, Berkeley, Spec. Publ. 1a.

Ludwig, K.R., 2000. SQUID 1.00: A User's Manual. Berkeley Geochronology Center, Berkeley, Spec. Publ. 2.

Mekhonoshin, A.S., Ernst, R., Söderlund, U., Hamilton, M.A., Kolotilina, T.B., Izokh, A.E., Polyakov, G.V., Tolstykh, N.D., 2016. Relationship between platinum-bearing ultramafic–mafic intrusions and large igneous provinces (exemplified by the Siberian Craton). Russian Geology and Geophysics (Geologiya i Geofizika) 57 (5), 822–834 (1043–1057).

Neimark, L.A., Larin, A.M., Nemchin, A.A., Ovchinnikova, G.V., Rytsk, E.Yu., 1998. Geochemical, geochronological (U–Pb), and isotope (Pb, Nd) evidence for anorogenic magmatism in the North Baikal volcanoplutonic belt. Petrologiya 6 (4), 139–164.

Okrugin, A.V., Beryozkin, V.L., Oleinikov, B.V., Savvinov, V.T., 1995. Late Precambrian dyke swarms of the Aldan Shield, Siberian Platform, in: Proceedings of the Third International Dyke Conference, Jerusalem, Israel, September 4–8,1995, p. 50.

Panteeva, S.V., Gladkochoub, D.P., Donskaya, T.V., Markova, V.V., Sandimirova, G.P., 2003. Determination of 24 trace elements in felsic rocks by inductively coupled plasma mass spectrometry after lithium metaborate fusion. Spectrochim. Acta, Part B 58, 341–350.

Pearce, J.A., 2008. Geochemical fingerprinting of oceanic basalts with applications to ophiolite classification and the search for Archean oceanic crust. Lithos 100 (1–4), 14–48.

Popov, N.V., Kotov, A.B., Postnikov, A.A., Sal'nikova, E.B., Shaporina, M.N., Larin, A.M., Yakovleva, S.Z., Plotkina, Yu.V., Fedoseenko, A.M., 2009. Age and tectonic position of the Chiney layered massif, Aldan Shield. Dokl. Earth Sci. 424 (1), 64–67.

Popov, N.V., Kotov, A.B., Sal'nikova, E.B., Postnikov, A.A., Timofeev, V.F., Berezkin, V.I., Larin, A.M., Fedoseenko, A.M., Yakovleva, S.Z., 2012. Kuranakh complex diabases in the western part of the Aldan–Stanovoi Shield: age and tectonic setting. Dokl. Earth Sci. 442 (1), 45–48.

Rosen, O.M., 2003. The Siberian craton: tectonic zonation and stages of evolution. Geotectonics 37 (3), 175–192.

Sharpenok, L.N., Kostin, A.E., Kukharenko, E.A., 2013. Total-alkali–silica (TAS) diagram for chemical classification and identification of intrusive rocks. Regional'naya Geologiya i Metallogeniya, No. 56, 40–50.

Shokhonova, M.N., Donskaya, T.V., Gladkochub, D.P., Mazukabzov, A.M., Paderin, I.P., 2010. Paleoproterozoic basaltoids in the North Baikal volcanoplutonic belt of the Siberian craton: age and petrogenesis. Russian Geology and Geophysics (Geologiya i Geofizika) 51 (8), 815–832 (1049–1072).

Steiger, R.H., Jäger, E., 1977. Subcommission on Geochronology: convention on the use of decay constants in geo- and cosmochronology. Earth Planet. Sci. Lett. 36 (3), 359–362.

Sun, S.-S., McDonough, W.F., 1989. Chemical and isotopic systematics of oceanic basalts: implications for mantle composition and processes Basins, in: Saunders, A.D., Norry, M.J. (Eds.), Magmatism in the Ocean Basins. Geol. Soc. London, Spec. Publ. Vol. 42, pp. 313–345.

Turkina, O.M., Kapitonov, I.N., 2017. Lu–Hf isotope composition of zircon as an indicator of the sources for Paleoproterozoic collisional granites (Sharyzhalgai uplift, Siberian craton). Russian Geology and Geophysics (Geologiya i Geofizika) 58 (2), 149–164 (181–199).

Turkina, O.M., Kapitonov, I.N., 2019. The sources of Paleoproterozoic collisional granitoids (Sharyzhalgai uplift, southwestern Siberian craton): from lithospheric mantle to upper crust. Russian Geology and Geophysics (Geologiya i Geofizika) 60 (4), 414–434 (489–513).

Turkina, O.M., Nozhkin, A.D., Bayanova, T.B., 2006. Sources and formation conditions of early Proterozoic granitoids from the southwestern margin of the Siberian craton. Petrology 14 (3), 262–283.

Wakita, H., Schmitt, R.A., Rey, P., 1970. Elemental abundances of major, minor, and trace elements in Apollo 11 lunar rocks, soil and core samples, in: Proceedings of the Apollo 11 Lunar Science Conference, Houston, Texas, January 5–8, 1970. Pergamon Press, New York, USA, pp. 1685–1717.

Wiedenbeck, M., Alle, P., Corfu, F., Griffin, W.L., Meier, M., Oberli, F., von Quadt, A., Roddick, J.C., Spiegel, W., 1995. Three natural zircon standards for U–Th–Pb, Lu–Hf, trace element and REE analysis. Geostand. Newslett. 19 (1), 1–23.

Williams, I.S., 1998. U–Th–Pb geochronology by ion microprobe, in: McKibben, M.A., Shanks, W.C. III, Ridley, W.I. (Eds.), Applications of Microanalytical Techniques to Understanding Mineralizing Processes. Rev. Econ. Geol. 7, 1–35.

Editorial responsibility: O.M. Turkina